Geochemical Perspectives Letters

Water driven iodine degassing from basaltic volcanic systems

H. Bureau, T. Grützner, A. Pakhomova, P. Munsch, I. Estève, Y. Guarnelli, J. Siebert, G. Garbarino, M. Mézouar

Supplementary Information

The Supplementary Information includes:

- Methods
- Tables S-1 and S-2
- Figures S-1 to S-4
- Supplementary Information References

Methods

Natural amounts of iodine in deep Earth's reservoirs (bulk silicate Earth, mantle rocks and basalts) are very low, in the order of magnitude of ppb (Guo and Korenaga, 2021). They cannot be detected *in situ* with X-Ray fluorescence and therefore, the starting samples must be doped with iodine contents high enough to be detectable by SRXF. To prepare the starting basaltic glass, we use a natural basalt powder (STV-301 from Saint-Vincent), pure water and sodium iodide loaded together in AuPd capsules. This mixture is melted at 1.1 GPa and 1300 °C for one hour in a piston cylinder apparatus at the Institut de Physique du Globe de Paris. The composition of the starting glass is checked for absence of crystals and for its chemical homogeneity with electron microprobe analysis at Camparis, Sorbonne Université (see Table S-1).
The fact that the initial iodine content of the basaltic magma is much higher than that observed in nature is not problematic because we measure a partition coefficient: a ratio independent of the initial iodine content assuming that the iodine partition coefficients are following Henry's law. It is also necessary to dope the experiments to wt. % level of Iodine in order to be able to be detected by SRXF.
This ratio is then used to calculate the iodine flux, assuming realistic initial iodine concentrations based on measurements taken in natural glasses and magma inclusions

To study degassing under anhydrous conditions, the iodine-bearing basaltic glass and a ruby sphere are manually loaded into pressure membrane diamond anvil cells DAC (Grützner *et al.*, 2024). CO_2 is loaded into the sample chamber using a DAC-gas loading system at IMPMC Paris, France (Figure 1, S-2). CO_2 also serves as the anhydrous fluid phase and as a pressure medium. During the experiments, external heating is provided by an external furnace ring at 250 °C only to ensure thermal convection in the DAC sample chamber. In these experiments only the melt phase is heated to high temperature, with the coexisting CO_2 fluid remaining at 250 °C.

For experiments performed under hydrous conditions, the iodine-bearing basaltic glass and a ruby sphere are manually loaded in the DAC with water as the pressure medium and as a fluid phase that will be in equilibrium with the melt at high temperature. In this case we use internally heated hydrothermal diamond

anvil cells (Grützner *et al*., 2024), capable of reaching 1100 °C in the whole sample chamber (Bureau *et al*., 2016). Ruby spheres are used for in situ pressure monitoring throughout the processes (Grützner *et al*., 2024). The pressure during the experiments is monitored with an automatic pressure controller connected to the pressure membrane of the DAC. For each pressure (P from 0.3 to 1.9 GPa and room pressure) and temperature step (T from 1300 to 1660 °C and room temperature) iodine is measured in the fluid and in the basaltic melt by Synchrotron X-Ray Fluorescence (SXRF) analysis (the setup is presented in the Figure S-1).

Laser heating is used for both series of experiments (CO_2 and H_2O), in addition to the external heating, using a YAG laser. We use a 50 µm defocused spot to reach the liquidus of the basaltic glass in a volume large enough to be analysed by the 2x2 μm^2 beam without any contamination of one phase by the other, especially the melt phase.
In the Id27 beamline, a double-sided laser heating system is optimized using focusing optics that produce a large and homogenous heated area. The system is composed of two motorised achromatic Schwarzschild objectives for sample visualisation and temperature measurements (see Mezouar *et al*., 2024). The temperature is measured on both sides of the diamond anvil cell. The temperature measurement is performed by spectral radiometry, by collecting the Planck radiation emitted by the sample. The accuracy is of less than 100 °C.

The new laser heating system for the Id27 beamline is highly stable and allows for continuous heating over several hours. For each experiment, laser heating for at least 30 minutes was performed before any SXRF chemical measurements to ensure chemical equilibrium. Before starting the SXRF analyses the absence of crystals in the melt is controlled with situ X-Ray diffraction (XRD). The new ID27 beam line functionality allows for the simultaneous analysis of the heating spot (in the melt) and the fluid that is in equilibrium with this melt. The high flux 46.834 KeV, 2x2 μm^2 photon beam is additionally scanned over the sample for at least 30 sec/point for micro-analysis and maps (from 20 to 500 µm on each side).

For the chemical measurement of iodine concentrations in the melt and in the fluid, we use only the 2x2μm^2 beam analysis. Maps are used to assess the overall iodine distribution before, during and after the experiments (Figure S-3). Iodine concentrations are calculated from the SXRF spectra using PyMCA software (Sole *et al*., 2007), as explained in our previous study (Bureau *et al*., 2016) from the Kα and Kβ rays of iodine (Figure 2). The accuracy of the analysis is verified by analysing double-polished glass plates of international standards (NIST610, NIST612) and well-known I-bearing glasses (Table S-1).
The iodine concentration is measured by transmission in situ in the DAC, this concentration depends on the thickness of the phase analysed.
The concentration of the starting basaltic glass is 1.14 wt. % I (± 0.03)
The thickness of the gasket is measured after the DAC is open, then the fluid concentration is always measured accurately, because the fluid thickness is known.
It is more difficult to measure the content of the melt for experiments performed in CO_2. The thickness of the starting glass pieces loaded in the DAC is known in because we use double-polished thin sections of the basaltic glass. This thickness changes when the glass is melted by laser and becomes round (globule of melt), and it is nearly impossible to measure it in situ during laser heating. This may be the reason why mass balance is note always observed in the Table 1 (experiments HAKA, EMMA, MARINA).
For the experiments H10 the mass balance is correct: total I 7870 ppm ± 1574 = 9452 ppm I.
For the experiment LN2, performed in water, the globule of melt is touching both diamond anvils, the mass balance is correct: total I 7877 ppm I ± 1575 = 9452 ppm I.

As detailed in Grützner *et al.*, 2024, we can calculate an annual bromine flux q_I:

$$q_I = (Q \times \rho B) / C_{fluid}$$

with ρB as the density for basalt (2.8 g/cm3). For the annual magma flux Q, we do not use the global arc magma flux of 2.5×10^{15} cm3/y, but the value corresponding to the erupted (i.e. effusive) magmas: the annual

global addition in volcanic material brought to the Earth's surface along 35,000 km of arc which varies between 0.14 and 0.9 $\times 10^{15}$ cm^3/y (Carmichael, 2002), we use 0.9 $\times 10^{15}$ cm3/y.
The iodine concentration in the fluid/degassing phase C_{fluid} can be calculated as:

$$C_{fluid} = C_{mi}.W.(D_{iodine}^{f/m} /(D_{iodine}^{f/m} + 1))$$

with C_{mi} as iodine concentration in melt inclusions and $D_{iodine}^{f/m}$ as the newly gained partition coefficient for aqueous fluid experiments from this study.
The addition of the factor W considers that the fluid fraction in our experiments is higher than in natural systems: Experiments from this study have a fluid fraction of 25 to 45 wt. %. Arc magmas can have water contents up to 20 wt. %, but probably not all over the globus (Urann *et al.*, 2022). Assuming a water content between 5 and 12 wt. % would lead to a factor W = 3 to 7.

Supplementary Tables

Table S-1 chemical compositions of the starting I-doped basaltic glass STV from Saint Vincent Lesser Antilles (Pichavant *et al.*, 2002), glassy standards C7, PC89 (Leroy *et al.*, 2019), V1 (Mosbah *et al.*, 1995). The I-doped STV glass was synthesized in the Institut de Physique du Globe de Paris, France, at 1.1 GPa, 1300 °C during 60 minutes in a piston cylinder apparatus and quenched at room conditions. NIST610, NIST612, trace elements compositions are after Rocholl *et al.*, (1997). Glasses compositions are calculated from SXRF spectra using the PyMCA Software (Solé *et al.*, 2007).

	STV basalt	Standard C7	Standard PC89	Standard V1
SiO_2	44.93	45.72	48.51	72.34
MgO	10.91	11.85	12.23	
Al_2O_3	14.72	14.94	16.04	13.73
MnO	0.12	0.17	0.17	
FeO	7.82	8.51	5.77	
TiO_2	1.14	1.13	1.25	
CaO	10.41	2.60	11.09	
Cr_2O_3	0.08	0		
K_2O	0.52	0.32	0.36	
Na_2O	2.40	2.60	2.88	13.93
NiO	0.02			
P_2O_5	0.12			
I	1.14 (±0.03)*	0.48 (±0.07)**	1.02 (±0.17)**	
H_2O	3.85 (±0.36)	3.97 (0.6)	0.13 (±0.02)	
Zn ppm				595 (±15)
As ppm				958 (30)
Zr ppm				1057 (50)
Total	98.38	100.34	99.45	100

Iodine contents are measured by *EMPA, based on 10 analyses, following the protocol defined in Grützner *et al.* (2017) and **PIXE following the protocol defined in Leroy *et al.* (2019). Water contents are measured by ERDA following the procedure described in (Bureau *et al.*, 2009).

Table S-2 SEM-EDX semi-quantitative chemical analysis in wt. % elements of the volatile-rich glassy quenched samples. Analysis are performed by energy-dispersive X-ray spectroscopy (EDX) in conjunction with the SEM. The detector was calibrated with a pure copper target at the beginning of each session to determine the beam current. EDX analyses were calibrated using international ASTIMEX® standards for spectral deconvolution and quantification. The resulting precision on the chemical analyses was about 1 wt. %. Analysis are not normalized, due to the presence of high water or CO_2 contents.
Samples and location of the analysis are shown in Figure S-2. Water is not analyzed.

	EMMA		H10	HAKA			MARINA		LN2
	G	**HS**	**HS**	**HS**	**G/C**	**G/C**	**G**	**HS**	**Bulk**
Si	16.78	9.46	19.09	35.32	24.51	28.69	21.38	12.15	18.63
Al	8.32	11.81	6.82	0.47	0.17	0.78	7.48	7.10	7.76
Mg	6.84	7.52	5.91	0.65	0.25	0.55	6.28	7.44	7.07
K	0.93	nd	0.37	0.20	nd	0.41	0.45	0.12	0.3
Ca	7.00	4.05	7.05	0.36	11.37	11.9	8.15	5.05	7.95
Ti	0.69	0.66	0.52	nd	nd	nd	0.62	0.52	0.74
Fe	5.85	6.88	5.49	0.64	0.51	1.29	6.58	4.64	8.09
Na	1.23	0.25	nd	nd	nd	0.21	1.43	0.57	1.63
Mn	0.09	0.09	nd	nd	nd	nd	0.06	0.07	0.12
Cr	nd	0.17	nd	nd	nd	0.19	nd	nd	nd
Cl	0.05	nd	nd	nd	0.25	nd	nd	nd	nd
I	**0.71**	nd	**0.81**	nd	nd	**1.43**	**1.13**	nd	NA
C	20.26	15.23	nd	9.76	12.87	nd	nd	22.95	nd
O	21.75	40.74	35.33	41.74	43.40	30.84	29.65	24.02	36.36
Total	76.2	101.38	82.73	89.22	93.33	76.29	86.21	84.77	88.69

G: Glass not melted but close to hot spot. HS: Hot Spot (laser heated in situ). G/C: glass + crystals. Bulk: bulk composition. NA Not Analyzed. nd not detected

Table S-3 Results obtained from in situ experiments in DAC. Iodine partition coefficient at extreme conditions. This study and *Bureau *et al.*, 2016)

Run	**Fluid**	**T °C**	**P GPa**	**$D^{I}_{f/m}$**
HAKA	CO_2	1391	0.89	0.001
EMMA	CO_2	1324	1.6	0.21
MARINA	CO_2	1400	1.9	0.09
H10	CO_2	1500	1	0.028
LN2	H_2O	800	1.52	0.86
#1*	H_2O	910	1.76	5.35
	H_2O	845	1.63	3.88
#2*	H_2O	900	1.12	6.76
	H_2O	844	1.03	9.14
#3*	H_2O	820	0.6	3.53
	H_2O	820	0.6	3.57
	H_2O	750	0.52	20
	H_2O	700	0.47	19
	H_2O	580	0.34	27
#4*	H_2O	570	1.08	5.55
#5*	H_2O	802	1.44	3.06
#6*	H_2O	794	1.51	1.92
	H_2O	697	1.32	2.94
	H_2O	697	1.32	3.15
#7*	H_2O	740	1.4	1.93
	H_2O	630	1.17	7.45
#8*	H_2O	640	1.2	5.26
#9*		600	0.17	34.9
		480	0.1	41

Supplementary Figures

Figure S-1 Photograph of the experimental setup at ID27. ESRF. The diamond anvil cell is aligned with the 2*2 µm Xray beam of 46.834 KeV. Fluorescence acquisition is performed thanks to a Vortex SDD detector equipped with a silicon poly-capillary that reduces the X-Ray background. Thanks to the setup XRD and XRF maps up to 100*100 µm are performed simultaneously while the DAC (Munsch *et al*., 2015 Chervin *et al*., 1995) is laser heated at HT on both sides (Mezouar *et al*., 2024).

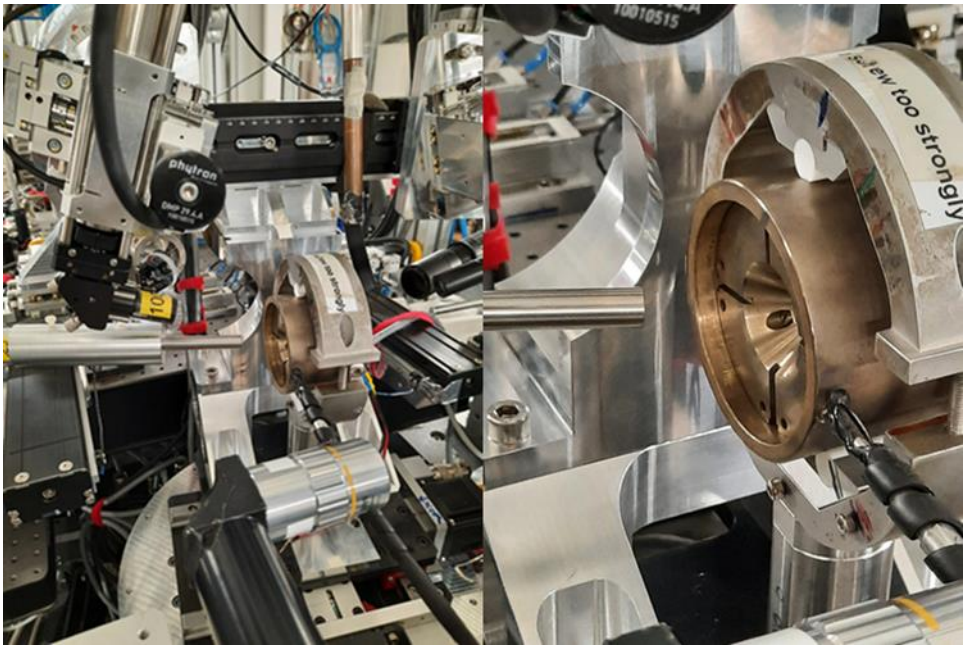

Figure S-2 Experiments performed in situ in DAC. A: H10. B: MARINA. C: EMMA. D: HAKA. E: LN2. All sample chambers diameter are of 500 µm. First column: pictures of the starting sample chamber before heating**.** Second column: pictures of the sample chambers after heating under pressure (Table S-3). Third column: SEM images of the quenched glasses at room conditions after the experiments. compositions are given in Table S-2. The red squares correspond to EDX analysis in Table S-2.

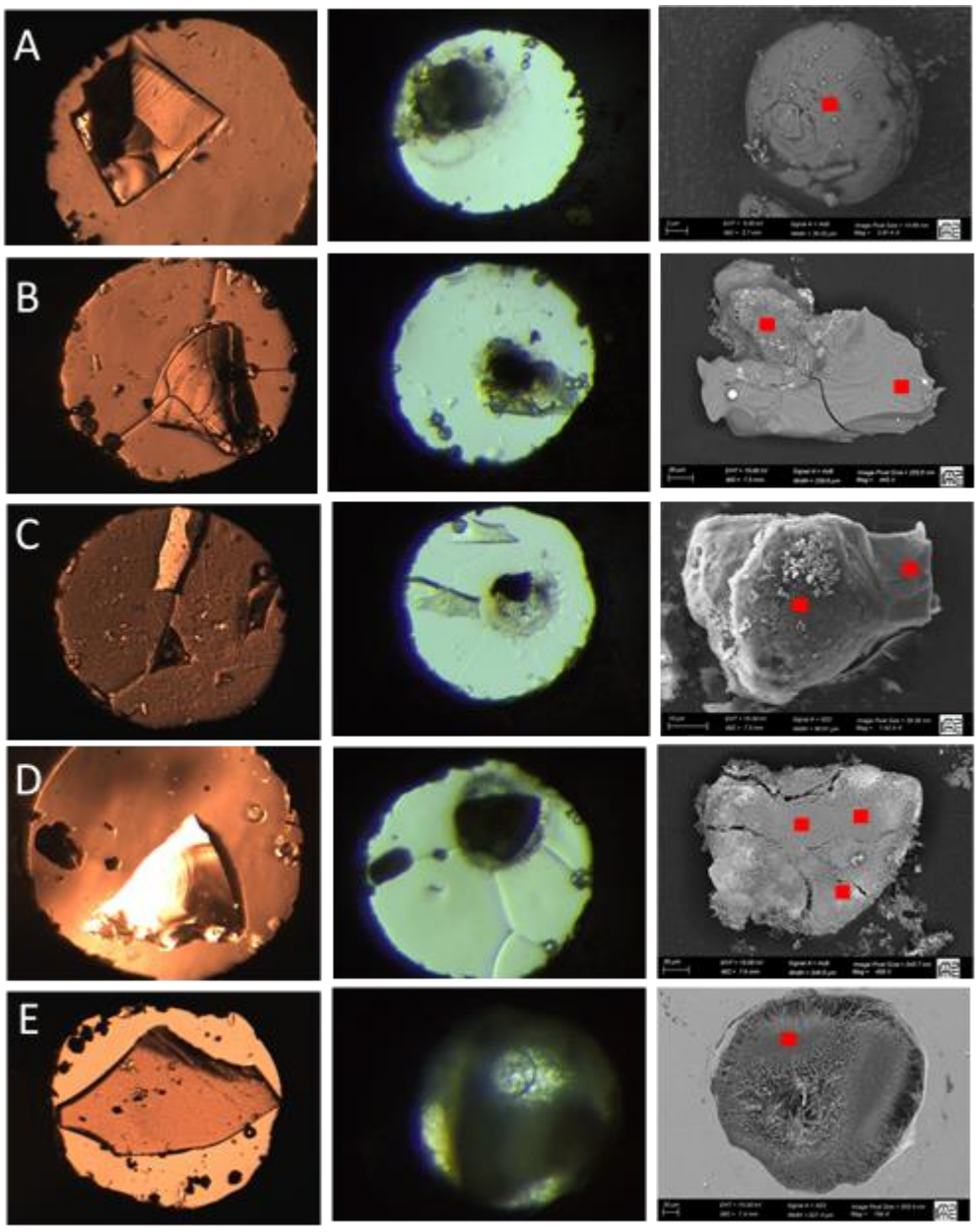

Figure S-3 left: In situ SXRF elemental maps of iodine distribution in the whole sample chambers of the DAC. at high pressure HP and room temperature RT after the experiments performed in CO_2 fluid (solid at RT). Right: pictures of the quenched DAC. Iodine is concentrated in the quenched pieces of glasses. preserved as globules (i.e. melted at HPHT). Diameter of the sample chambers is 500 µm. The circles delimit the melting points (50µm). Some pieces of glasses are not melted.

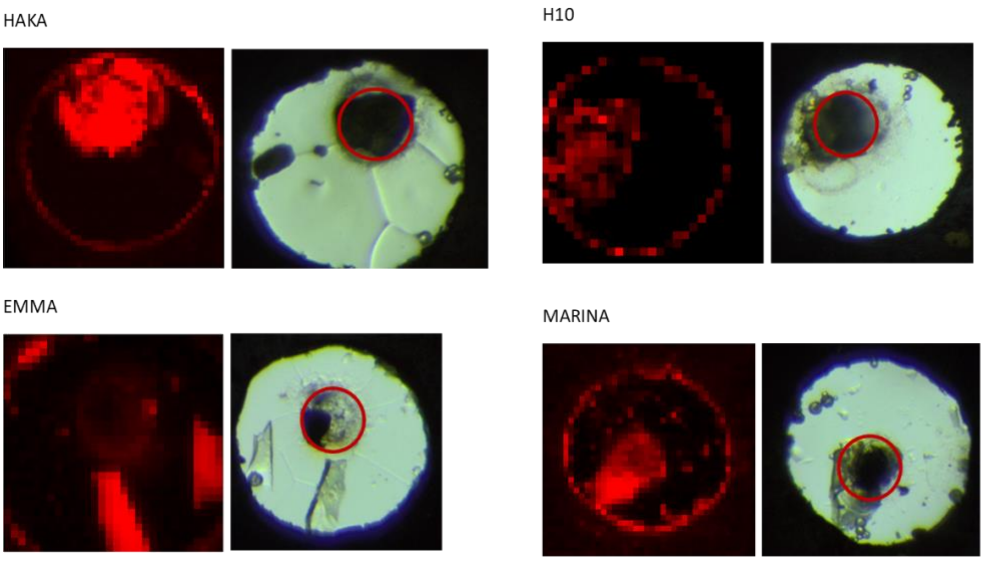

Figure S-4 Partition coefficients of iodine (purple) and bromine (green) determined in situ between melts and fluids (H_2O. CO_2 for iodine; H_2O Neon for bromine) in diamond anvil cells. Round symbols are for haplogranite melts (i.e. crustal melts, only in water): bold green circles are for bromine, open purple circles are for iodine. Square symbols are for natural basaltic melts. Bold squares are for CO_2 (iodine) or Neon (analogue for CO_2, bromine) fluids. Open squares are for H_2O fluids. Maximum error bars are shown with the upper right cross. Degassing of both iodine and bromine occurs in a lesser magnitude for dry magmatic fluids. The data confirm the much weaker effect of temperature on heavy halogens degassing than that of pressure.

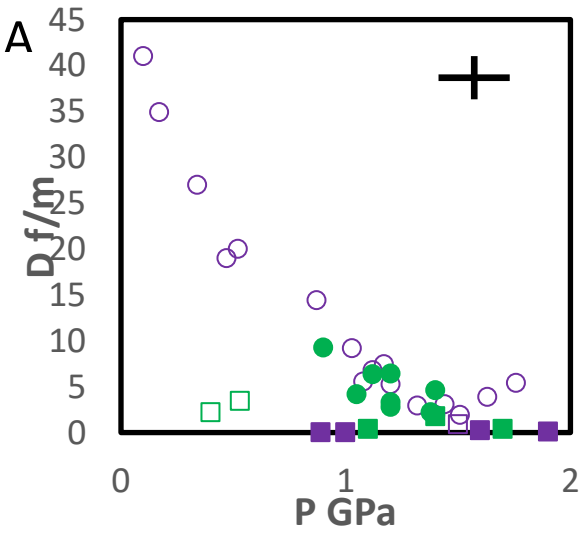

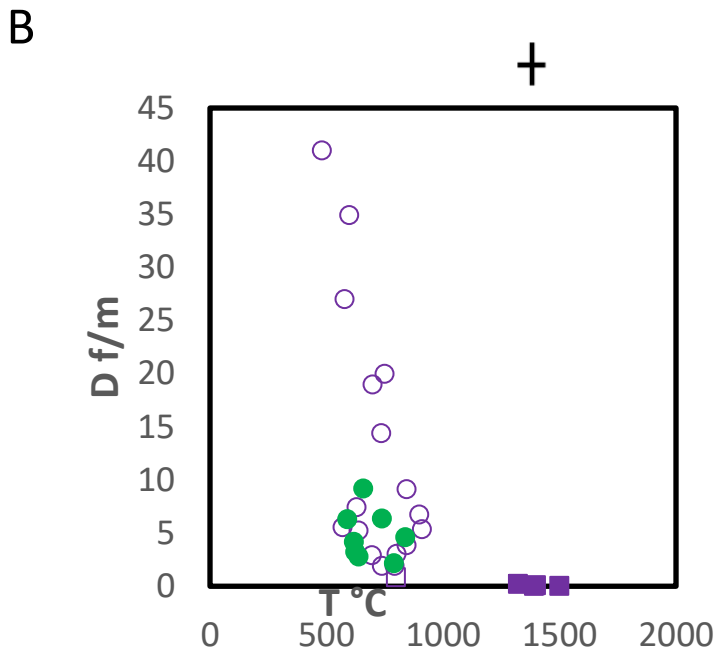

Figure S-5 Partition coefficients of iodine (purple) and bromine (green) determined in situ between melts and fluids (H_2O. CO_2 for iodine; H_2O Neon for bromine) in diamond anvil cells. See Figure 3 for legends. Different visualisation of the data: A LogD versus pressure and B LogD versus temperature.
A trend is observed between LogD and the temperature for very high values (T >1400 °C), confirming that iodine degasses during the decrease of both P and T.

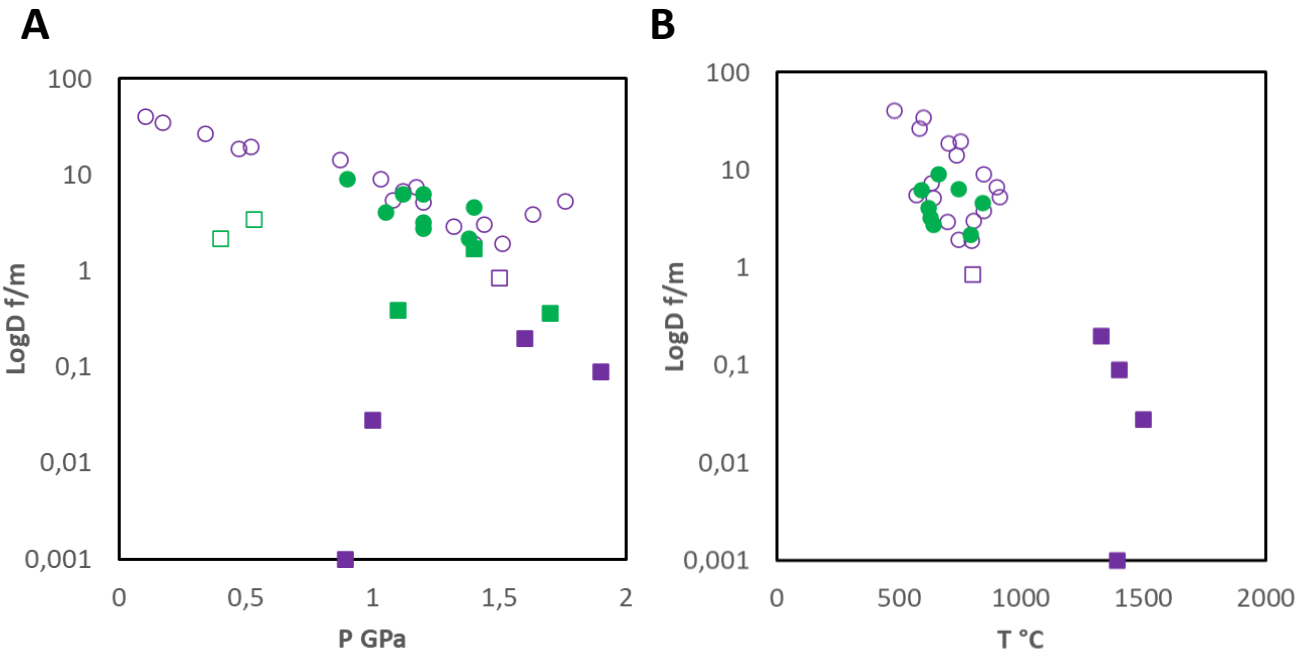

Supplementary Information References

Bureau, H., Raepsaet, C., Khodja, H., Carraro, A., Aubaud, C. (2009) Determination of hydrogen content in geological samples using Elastic Recoil Detection Analysis (ERDA). *Geochimica et Cosmochimica Acta* 73, 3311-3322. https://doi.org/10.1016/j.gca.2009.03.009

Bureau, H., Auzende, A.-L., Marocchi, M., Raepsaet, C., Munsch, P., Testemale, D., Mézouar, M., Kubsky, S., Carrière, M., Ricolleau, A., Fiquet, G. (2016) Modern and past volcanic degassing of iodine. *Geochimica et Cosmochimica Acta* 173, 114–125. https://doi.org/10.1016/j.gca.2015.10.017

Carmichael, I.S. (2002) The andesite aqueduct: perspectives on the evolution of intermediate magmatism in west-central (105–99°W) Mexico. *Contributions to Mineralogy and Petrology* 143, 641–663. https://doi.org/10.1007/s00410-002-0370-9

Chervin, J.C., Canny, B., Besson, J.M., Pruzan, P. (1995) A diamond anvil cell for IR microspectroscopy. *Rev. Sci. Instrum. 66*, 2595–2598. https://doi.org/10.1063/1.1145594

Guo, M., Korenaga, J. (2021) A halogen budget of the bulk silicate Earth points to a history of early halogen degassing followed by net regassing. *PNAS* 118, No. 51 e2116083118 https://doi.org/10.1073/pnas.2116083118

Grützner, T., Kohn, S.C., Bromiley, D.W., Rohrbach, A., Berndt, J. Klemme, S. (2017) The storage capacity of fluorine in olivine and pyroxene under upper mantle conditions. *Geochimica et Cosmochimica Acta* 208, 160-170. https://doi.org/10.1016/j.gca.2017.03.043

Grützner, T., Bureau, H., Boulard, E., Munsch, P., Guignot, N., Siebert, J., Guarnelli, Y. (2024) An in-situ experimental HP/HT study on bromine release from a natural basalt. *Chemical Geology* 644, 121869. https://doi.org/10.1016/j.chemgeo.2023.121869

Leroy, C., Bureau, H., Sanloup, C., Raepsaet, C., Glazirin, K., Munsch, P., Harmand, M., Prouteau, G., Khodja, H. (2019) Xenon and iodine behaviour in magmas. *Earth Planet. Sci. Lett.* 522, 144–154. https://doi.org/10.1016/j.epsl.2019.06.031

Mezouar, M., Garbarino, G., Bauchau, S., Morgenroth, W., Martel, K., Petitdemange, S., Got, P., Clavel, C., Moyne, A., Van Der Kleij, H.-P., Pakhomov, A., Wehinger, B., Gerin, M., Poreba, T., Canet, L., Rosa, A., Forestier, A., Weck, G., Datchi, F., Wilke, M., Jahn, S., Andrault, D., Libon, L., Pennacchioni, L., Kovalskii, G., Herrmann, M., Laniel, D., Bureau, H. (2024) The high flux nano-X-ray diffraction. fluorescence and imaging beamline ID27 for science under extreme conditions on the ESRF Extremely Brilliant Source. *High Pressure Research*. 44, 171–198. https://doi.org/10.1080/08957959.2024.2363932

Mosbah, M., Clocchiatti, R., Michaud, V., Piccot, D., Chevallier, P., Legrand, F., Als Nilsen, G., Grübel, G. (1995) Micro PIXE and micro SXRF: comparison of the two methods and application to glass inclusions from Vulcano (Eolian Islands – Italy). *Nucl. Inst. Methods Phys. Res. B* 104, 481–488. https://doi.org/10.1016/0168-583X(95)00472-6

Munsch, P., Bureau, H., El Yakoubi, M., Khodja, H., Zaitsev, A. (2015) The use of ^{13}C diamond as pressure and temperature sensor for diamond-anvil-cell experiments. *Eur. J. Mineral.* 27, 365–375. https://doi.org/10.1127/ejm/2015/0027-2439

Pichavant, M., Mysen, B.O., Macdonald, R. (2002) Source and H_2O content of high-MgO magmas in island arc settings: an experimental study of a primitive calc-alkaline basalt from St. Vincent. Lesser Antilles arc. *Geochim. Cosmochim. Acta* 66, 2193–2209. https://doi.org/10.1016/S0016-7037(01)00891-2

Rocholl, A.B.E., Simon, K., Jochum, K.P., Gehann, R., Kramar, U., Luecke, W., Molzahn, M., Pernicka, E., Seufert, M., Spettel, B., Stummeier, J. (1997) Chemical characterization of NIST silicate glass certified reference material SRM 610 by ICPMS. TIMS. LIMS. SSMS. INAA. AAS and PIXE. *Geostand. Newslett.* 21-1, 101–114. https://doi.org/10.1111/j.1751-908X.1997.tb00537.x

Solé, A., Papillon, E., Cotte, M., Walter, Ph., Susini, J. (2007) A multiplatform code for the analysis of energy-dispersive X-ray fluorescence spectra. *Spectrochim. Acta. Part B* 62, 63–68. https://doi.org/10.1016/j.sab.2006.12.002

Urann, B.M., Le Roux, V., Jagoutz, O., Müntener, O., Behn, M.D., Chin, E.J. (2022) High water content of arc magmas recorded in cumulates from subduction zone lower crust. *Nat. Geosci.* 15, 501–508. https://doi.org/10.1038/s41561-022-00947-w